Multiple brain activation patterns for the same task

Johan Nakuci[1*], Jiwon Yeon[2], Nadia Haddara[1], Ji-Hyun Kim[3], Sung-Phil Kim[3] and Dobromir Rahnev[1]

[1]School of Psychology, Georgia Institute of Technology, Atlanta, Georgia, 30332, USA.
[2]Department of Psychology, Stanford University, Stanford, California, 94305, USA.
[3]Department of Biomedical Engineering, Ulsan National Institute of Science and Technology, Ulsan, South Korea.

*Corresponding author. Email: jnakuci@gmail.com

Keywords: perceptual decision making, clustering, fMRI, default mode network

Acknowledgments: This work was supported by the National Institutes of Health (grant R01MH119189 to DR) and the Office of Naval Research (grant N00014-20-1-2622 to DR).

Competing interests: Authors declare that they have no competing interests.

Author contributions:
Conceptualization: JN, DR
Methodology: JN, JY, NH, DR
Data Curation: JY, NH, JHK, SPK
Visualization: JN, DR
Funding acquisition: DR
Writing – original draft: JN, DR
Writing – review & editing: JN, JY, NH, JHK, SPK, DR

Abstract

Meaningful variation in internal states that impacts cognition and behavior remains challenging to discover and characterize. Here we leveraged trial-to-trial fluctuations in the brain-wide signal recorded using functional MRI to test if distinct sets of brain regions are activated on different trials when accomplishing the same task. Across three different perceptual decision-making experiments, we estimated the brain activations for each trial. We then clustered the trials based on their similarity using modularity-maximization, a data-driven classification method. In each experiment, we found multiple distinct but stable subtypes of trials, suggesting that the same task can be accomplished in the presence of widely varying brain activation patterns. Surprisingly, in all experiments, one of the subtypes exhibited strong activation in the default mode network, which is typically thought to decrease in activity during tasks that require externally focused attention. The remaining subtypes were characterized by activations in different task-positive areas. The default mode network subtype was characterized by behavioral signatures that were similar to the other subtypes exhibiting activation with task-positive regions. Finally, in a fourth experiment, we tested whether multiple activation patterns would also appear for a qualitatively different, working memory task. We again found multiple subtypes of trials with differential activation in frontoparietal control, dorsal attention, and ventral attention networks. Overall, these findings demonstrate that the same cognitive tasks are accomplished through multiple brain activation patterns.

Introduction

Brain activity elicited by the same stimulus or task is highly variable[1,2]. Variation in task-induced brain activity has been identified in individual neurons[3] and large-scale brain networks[4] impacting cognition and behavior[5,6]. Variation in brain activity affects our actions in social situations[7], economic decisions[8], and even low-level perception[9].

Despite the widespread variability in brain activity during a task, standard analyses aim to identify the task-induced changes in brain activity across all trials[10]. Such analyses have been applied to a multitude of tasks such as face perception[11], memory[12], and navigation[13,14]. The prevailing assumption in studies seeking to identify the brain response to a stimulus or a task is that there is a single pattern of activation. In the case of fMRI, this pattern is typically identified by performing a standard general linear modeling analysis. Under this assumption, trial-to-trial variation in brain activity is simply noise. When applied to tasks that require *externally focused* attention, this standard analysis has identified a set of regions – termed "task-positive" – that increase in activity, and another set of regions – termed "task-negative" – that decrease in activity in response to external demands[15].

However, it is also possible that subsets of trials can produce meaningfully different patterns of activations that are not well captured by averaging across all trials. Indeed, the blood-oxygen level-dependent (BOLD) signal in fMRI is both spatially and temporally variable[16], with at least some of this variability likely to stem from meaningful variations in internal processing rather than simply noise[5,6,17,18]. Further, it has been hypothesized that a cognitive process can be accomplished through multiple pathways because of degeneracy[19], and supported by work utilizing theoretical models and patient populations[20], but these multiple pathways have not been explicitly identified in healthy individuals.

Here, we sought to identify discrete patterns of brain activity associated with the completion of the same task. To do so, we utilized a data-driven classification method to identify unique patterns in brain activity among individual trials. Across three perceptual-decision making experiments, we found multiple different activation patterns, with one of them surprisingly exhibiting task-negative activations. We further established the behavioral profile associated

with each subtype. Finally, we replicated the existence of multiple activations patterns in a working memory task. Overall, our results indicate that multiple brain activation patterns can co-exist in the context of the same task.

Results

Variation in brain activity across individual trials

We examined the patterns of brain activation produced across three perceptual decision-making tasks (Experiments 1-3) and in an *n*-back task from the Human Connectome Project[21] (**Table 1**). We first performed a standard GLM analyses to identify task-related brain activations. In Experiment 1, we observed increased activity in the visual and motor cortices, and decreased brain activity in the orbital frontal cortex and in the posterior cingulate cortex (**Fig. 1A**). However, single-trial beta responses estimated with a general linear model (GLM) using GLMsingle[22] deviated substantially from the group map. For example, unlike the group map, trial 2 for subject 1 showed strong positive activity in both the posterior cingulate cortex and the orbitofrontal cortex (**Fig. 1B**). On the other hand, trial 6 for subject 1 produced an activation pattern similar to the group map with negative activity in both the posterior cingulate cortex and the orbitofrontal cortex (**Fig. 1C**).

Table 1. Experiment details.

	Subjects	Total # of Trials
Experiment 1	50	35,682
Experiment 2	39	31,024
Experiment 3	40	9.959
HCP Working Memory	48	3,840

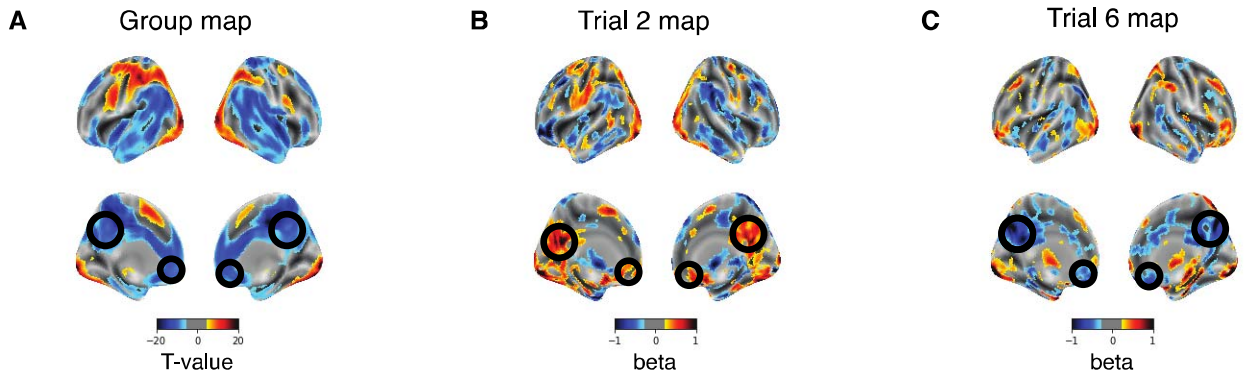

Figure 1. Variation in brain activity across individual trials in Experiment 1. (A) In Experiment 1, standard group analyses identified voxels with strong increases and decreases in task-induced brain activation across the cortex. The group brain map is thresholded at $P < 0.001$ for display purposes. Brain activation maps for (B) trial 6 and (C) trial 2 from subject 1 demonstrate substantial variability across trials that is not represented in the standard group brain map. Brain maps for the individual trials are thresholded at $|beta| > 0.25$ for display purposes. Black circles highlight the activation in the posterior cingulate cortex and orbitofrontal cortex.

<u>Multiple distinct but stable subtypes of trials during perceptual decision making</u>

The divergence in brain activity between the two trials and to the group map highlights the possibility that more than one pattern of brain activation may exist when performing a task. To test for this possibility, we utilized a data-driven classification method to determine if multiple unique patterns of activation emerge across trials. For each trial, we estimated the task-induced brain activity in each voxel and pooled trials across subjects. We estimated the similarity across the activations between pairs of trials using Pearson correlation and clustered all trials using modularity-maximization [23] to identify consistent activation patterns. Clustering produced three subtypes of trials in Experiment 1 (**Fig. 2A)**. Each subtype accounted for a roughly similar proportion of all trials and each subtype was present in all subjects and in each of the four stimulus conditions in that experiment (see Methods) (**Fig. 2B**).

Critically, we examined the pattern of activation present in each subtype. To do so, we averaged the trials from each subtype within a subject. We then performed a group-level one-sample t-test on the average beta values to identify voxels with significant positive or negative activations (using a threshold of FDR-corrected $P < 0.01$; **Fig. 2C**). In Experiment 1, we found that Subtype 1 was characterized by bilateral visual, parietal and left motor activations, as well as medial frontal, cingulate, temporal, and right motor deactivations. Subtype 2 had many similarities with

Subtype 1 – such as visual and parietal activations couple with medial frontal, cingulate, and anterior temporal deactivations – but featured strong bilateral activations in the insula (whereas Subtype 1 had bilateral deactivations in the insula). Subtype 3 had the most surprising profile with strong activations along the default mode network (DMN) and deactivations in a number of task-positive parietal and frontal areas. To further confirm these results, we also performed a standard GLM analysis with subtypes as factors in the regression and found similar patterns of activations (**Fig. S1**). Additionally, we performed the analysis within each of the four stimulus conditions separately to ensure that the subtypes do not simply reflect differences between conditions (**Fig. S2**). These results indicate the existence of multiple activation patterns within a task and one of the patterns exhibits strong DMN activation.

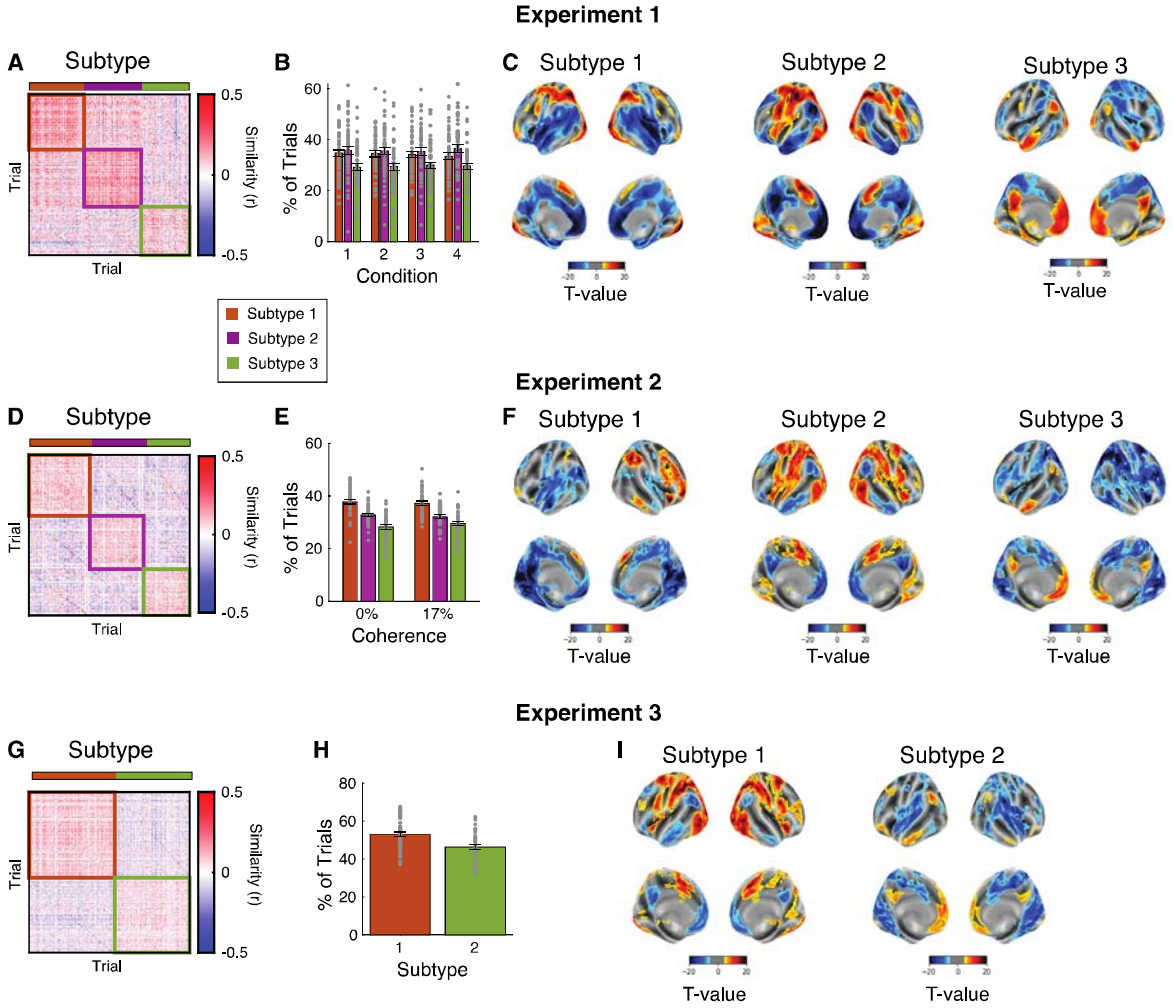

Figure 2. Subtypes of trials and activation maps in three perceptual decision-making tasks. (A-C) Results for Experiment 1. (A) Modularity-maximization based clustering identified three

subtypes of trials. The colored squares correspond to the trials composing each subtype. Pearson correlation was used to calculate the spatial similarity in activation (betas) among individual trials. (B) The percent of trials classified as Subtype 1, 2, and 3 for each of the four stimulus conditions. The dots represent individual subjects. (C) Activation maps for each subtype. Each activation map was calculated by first averaging the trials for each subtype within a subject, followed by one-sample t-test to identify regions in which brain activity increased or decreased in response to the task. Brain maps are thresholded at $P_{FDR\text{-}corrected} < 0.01$. (D-F) Results for Experiment 2. (D) Modularity-maximization clustering identified three subtypes of trials. (E) The percent of trials classified as Subtype 1, 2, and 3. (F) Activation maps for each subtype. (G-I) Results for Experiment 3. (G) Modularity-maximization clustering identified two subtypes of trials. (H) The percent of trials classified as Subtype 1 and 2. Note that Experiment 3 contained only a single condition. (I) Activation maps for each subtype.

To corroborate these findings, we performed the same analysis in two additional experiments that involved perceptual decision-making tasks – Experiments 2 and 3 (**Fig. 2D-I**). In Experiment 2, the group-level one-sample t-test on the average beta values identified voxels with significant positive and negative activations (FDR-corrected $P < 0.01$; **Fig. 2F**). Similar to Experiment 1, Subtypes 1 and 2 were characterized by activation across task-positive regions, whereas Subtype 3 exhibited strong activations in the DMN. In Experiment 3, clustering identified two subtypes. Similar to Experiments 1 and 2, the Subtype 1 exhibited activation in task-positive regions, whereas Subtype 2 exhibited strong activations in DMN (FDR-corrected $P < 0.01$; **Fig. 2I**). Taken together, these results confirm the existence of multiple activation patterns in three different experiments. Critically, in every experiment, one of the patterns exhibits activation in areas associated with the DMN, brain regions commonly thought to deactivate during tasks that require externally focused attention.

To better characterize the differences between the three subtypes, we directly compared the patterns of activation among each pair of subtypes. For Experiment 1, we found that relative to Subtype 1, Subtype 2 exhibited strongly increased activity in bilateral insula, together with a host of additional smaller differences in the frontal, parietal, and temporal lobes (paired-sample t-test; $P_{FDR\text{-}corrected} < 0.01$; **Fig. 3A**). On the other hand, compared to both Subtypes 1 and 2, Subtype 3 showed increased brain activity in the regions of the default mode network, including medial frontal cortex, posterior cingulate cortex, lateral parietal cortex, and anterior temporal cortex (paired-sample t-test; $P_{FDR\text{-}corrected} < 0.01$; **Fig. 3B, C**).

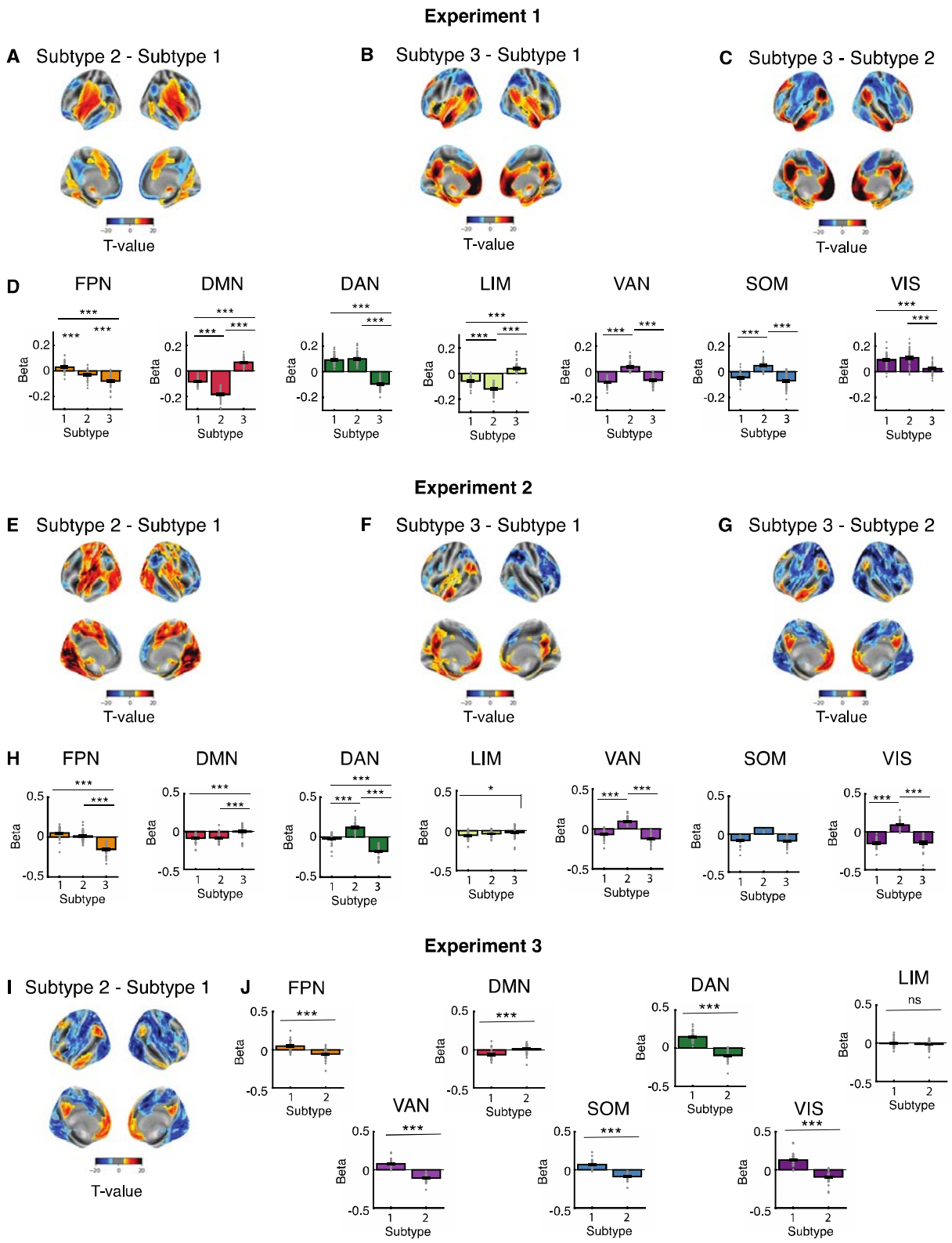

Figure 3. Activation differences between subtypes of trials. (A-D) Results for Experiment 1. Brain activation differences between (A) Subtype 2 and Subtype 1, (B) Subtype 3 and Subtype 1, and (C) Subtype 3 and Subtype 2. (D) Activation for each of seven large-scale brain networks for

each subtype. The bar graph shows the average change in activation (mean ± sem). The grey dots show the activation in each subject. (E-H) Results for Experiment 2. Brain activation differences between (E) Subtype 2 and Subtype 1, (F) Subtype 3 and Subtype 1, and (G) Subtype 3 and Subtype 2. (H) Activation for each of seven large-scale brain networks for each subtype. (I-J) Results for Experiment 3. (I) Brain activation differences between Subtype 2 and Subtype 1. (J) Activation for each of seven large-scale brain networks for each subtype. Differences between subtypes were estimated using a paired-samples t-test. Brain maps are thresholded at $P_{FDR\text{-}corrected} < 0.01$. * $P_{FDR\text{-}corrected} < 0.05$, *** $P_{FDR\text{-}corrected} < 0.001$, n.s., not significant. FPN, Frontal Parietal Network; DMN, Default Mode Network; DAN, Dorsal Attention Network; LIM, Limbic Network; VAN, Ventral Attention Network; SOM, Somatomotor Network; VIS, Visual Network.

To further understand the nature of each subtype, we examined the pattern of activation within established brain networks for each subtype. For each subject we averaged the voxels within each of the seven brain networks – frontoparietal network (FPN), default mode network (DMN), dorsal attention network (DAN), limbic network (LIM), ventral attention network (VAN), somatomotor network (SOM), and visual network (VIS) – defined in the Schaefer Atlas[23]. We found that Subtype 3 exhibited the strongest activations in DMN and the limbic networks but weakest activations in FPN, DAN, and the visual network (paired-samples t-tests; $P_{FDR\text{-}corrected}$; **Fig. 3D**). Compared to Subtype 2, Subtype 1 showed strong activation in FPN, DMN, and the limbic networks, but weaker activation in VAN and somatomotor networks. Interestingly, Subtypes 1 and 3 showed similar VAN and somatomotor activations, with both being significantly different from Subtype 2.

We performed the same analysis in Experiments 2 and found results broadly similar to Experiment 1 (paired-sample t-test; $P_{FDR\text{-}corrected} < 0.01$; **Fig. 3E-H**). Critically, Subtype 3 showed increased brain activity in the regions of the DMN compared to Subtypes 1 and 2 (paired-sample t-test; $P_{FDR\text{-}corrected} < 0.01$). Lastly, Experiment 3 further confirmed the increased brain activity in the regions of the DMN for Subtype 2 compared to Subtype 1 (paired-sample t-test; $P_{FDR\text{-}corrected} < 0.01$; **Fig. 3I-J**).

<u>Brain regions exhibiting consistent activation across subtypes</u>

In addition to exploring the differences between the subtypes, we also examined what is common across them. To identify areas exhibiting consistent activations or deactivations in brain activity

across the three subtypes, we identified the voxels in which the sign of activation was consistent among subtypes. Specifically, for each subtype, we binarized the brain maps for each subtype and averaged across subjects to identify the areas of spatial overlap among all subtypes. We found consistent activations in the visual and left motor cortex, as well as consistent deactivations in medial somatomotor, right motor, and bilateral temporal cortex (**Fig. 4**).

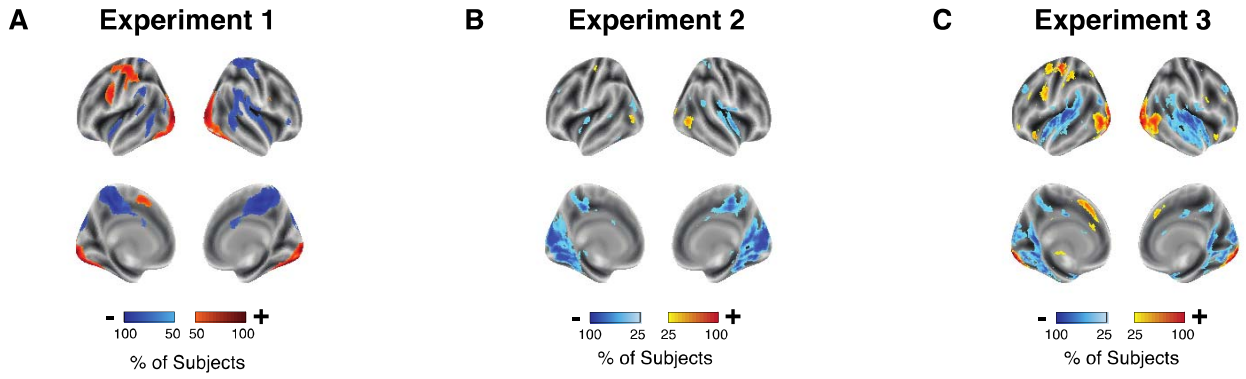

Figure 4. Consistency across the subtypes. Voxels exhibiting consistent activation in all subtypes in (A) Experiment 1, (B) Experiment 2, and (C) Experiment 3. The activation maps for each subtype were binarized to identify the areas of spatial overlap among all subtypes. For visualization purposes, maps are threshold at 50% of subjects in Experiment 1 and 25% of subjects in Experiments 2 and 3.

<u>Behavioral differences between subtypes</u>

Having identified these three different subtypes of trials in Experiment 1, we investigated how they affected behavioral performance. We compared how behavioral performance differed among subtypes using a mixed-effect model to account for the different conditions within the experiments. The model assessed the effects of subtype and condition with the subject as a random factor on behavioral performance. For Experiment 1, significant effects of subtype were present for reaction time (RT) ($t(35679) = 2.90$, $P = 0.004$) and confidence ($t(35679) = -3.37$, $P = 0.001$), but not accuracy ($t(35679) = -1.78$, $P = 0.07$; **Fig. 5A**). Additionally, the correlation between behavioral measures (accuracy, RT, and confidence) and brain activation improved for each subtype compared to when all trials were considered together, suggesting that considering each subtype separately increases the sensitivity in brain-behavior relationship (**Fig. S3-S5**).

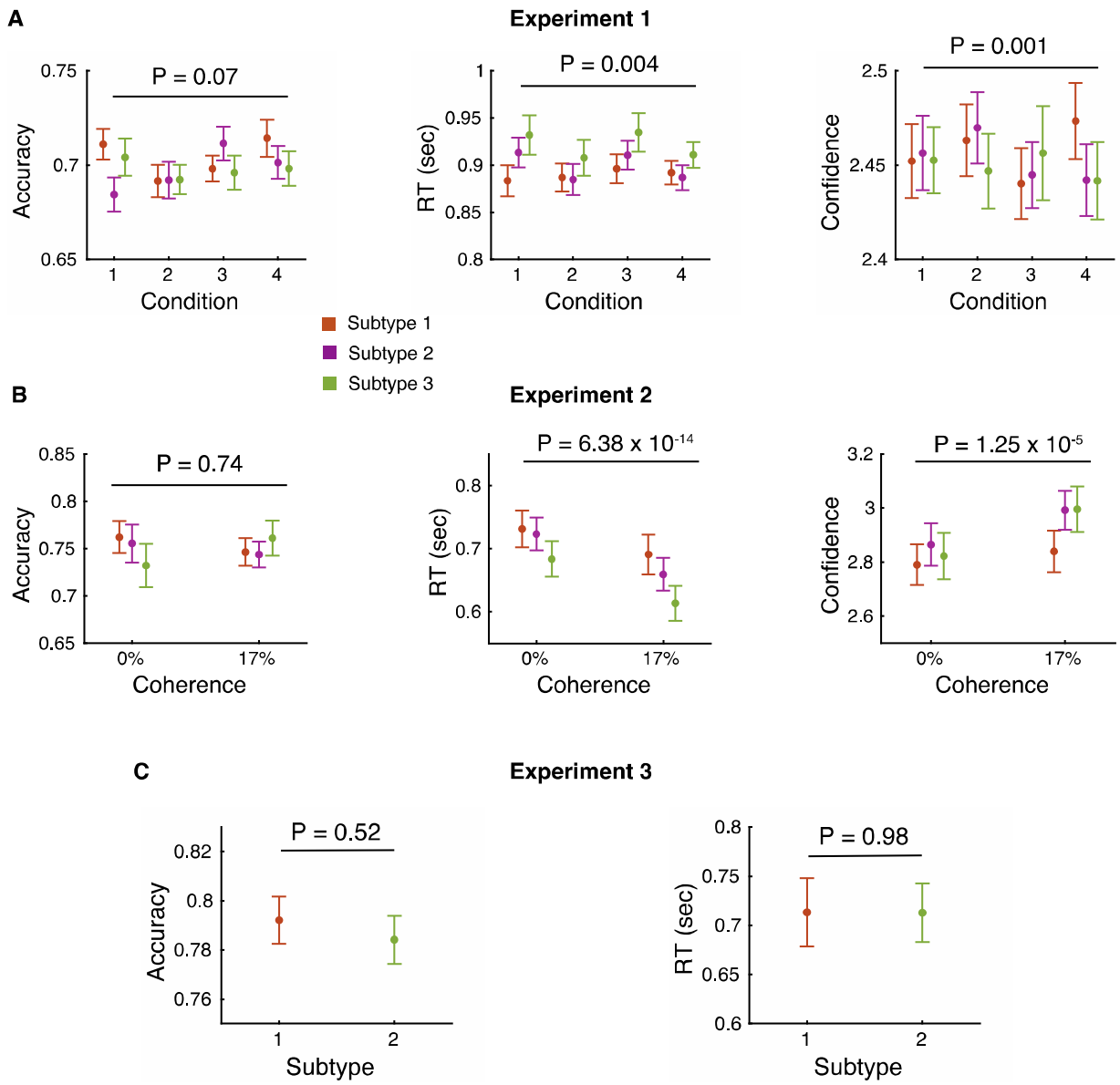

Figure 5. Behavioral differences between subtypes. Differences between subtypes in accuracy, RT, and confidence for (A) Experiment 1, (B) Experiment 2, and (C) Experiment 3. Note that Experiment 3 contained only a single condition and confidence was not measured. Statistical testing was conducted using linear mixed-effect model where the effects of subtype and condition with the subject as a random factor on behavioral performance. P-values show the effect of subtype on behavioral performance. Error bars show SEM.

The same analyses for Experiment 2 uncovered significant differences in RT ($t(30351) = -4.99$, $P = 5.83 \times 10^{-7}$) and confidence ($t(30351) = 4.37$, $P = 1.25 \times 10^{-5}$), but not accuracy ($t(30351) = 0.33$, $P = 0.74$; **Fig. 5B**). Interestingly, and in contrast to Experiment 1, in Experiment 2, the

fastest RTs were associated with Subtype 3, which showed activation in the DMN. Lastly, in Experiment 3, there were no significant difference in accuracy or RT between subtypes ($P > 0.05$; **Fig. 5C**). (Note that confidence was not measured in the Experiment 3.) Overall, the differences in accuracy, RT, and confidence were small and their direction was sometimes inconsistent between studies, suggesting that the subtypes do not simply reflect differences in task difficulty or other stimulus characteristics.

Identification of trial subtypes is robust

To test the robustness of the subtypes, we performed a 2-fold cross-validation analysis using support vector machine (SVM) classifier. Specifically, we trained an SVM classifier on the subtype labels in half the data and tested its ability to predict the correct subtype labels in the remaining half of the data. We found that the SVM classifier correctly predicted subtype labels on 94.8% of the trials in Experiment 1, 95.6% of the trials in Experiment 2, and 97.8% of trials in Experiment 3, thus confirming the robustness of the three subtypes (**Fig. 6**).

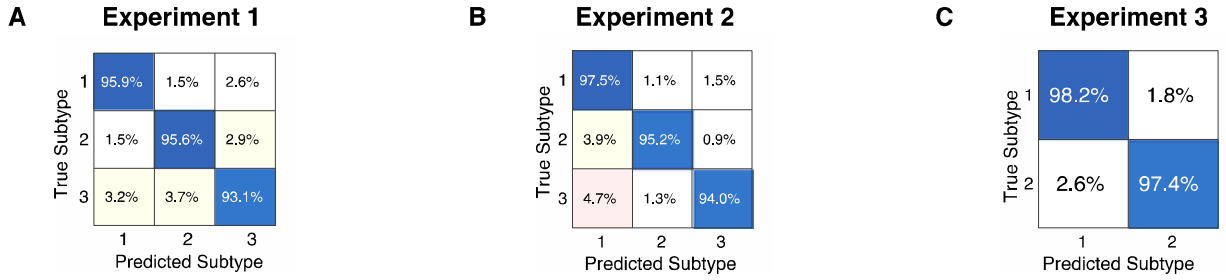

Figure 6. SVM classification. Confusion matrix showing SVM classification accuracy for (A) Experiment 1, (B) Experiment 2, and (C) Experiment 3. SVM classification was based on 2-Fold cross-validation analysis.

Multiple distinct but stable subtypes of trials during working memory task

The analyses thus far focused on three perceptual decision-making experiments. However, finally, we also examine if multiple activation patterns exist in a different cognitive task. Specifically, we analyzed the *n*-back task data from the Human Connectome Project where subjects completed equal number of 0- and 2-back trials[21]. In the same manner as for

Experiments 1-3, for each trial we estimated the task-induced brain activity in each voxel and pooled trials across subjects and *n*-back conditions, and then clustered the trials using modularity-maximization. Clustering identified three robust subtypes (**Fig. 7A**) present all subtypes were present in both the 0- and 2-back conditions, but Subtype 1 was primarily in 0-back and Subtype 2 was primarily in the 2-back condition (**Fig. 7B**). Further, as in Experiments 1-3, the SVM classifier correctly labeled 87.4% of trials highlighting the robustness of the subtypes (**Fig. 7C**). Examining the brain activation patterns, the visual network exhibited consistent activation in all three subtypes (**Fig. 7D**). Critically, the three subtypes exhibited differences in activation at the voxel level and among large-scale networks as in Experiments 1-3. We found that Subtype 2 relative to Subtype 1 and Subtype 3, exhibited stronger activation in the FPN and strong deactivation in the somatomotor regions (paired-sample t-test; $P_{FDR\text{-}corrected} < 0.01$; **Fig. 7E**). On the other hand, compared to both Subtypes 1 and 2, Subtype 3 showed increased brain activity in brain region associated with the VAN and somatomotor network (paired-sample t-test; $P_{FDR\text{-}corrected} < 0.01$; **Fig. 7F**). Additionally, we performed the analysis within each condition separately to ensure that the subtypes do not represent differences between the two *n*-back conditions, and we found the same patterns of activation within the 0- and 2-back separately (**Fig. S6).** Further, we examined if there were behavioral differences between subtypes using a mixed-effect model as in the working memory task and we found significant differences in accuracy ($t(3837) = 2.74$, $P = 0.006$) but not for RT ($t(3837) = 0.23$, $P = 0.82$) (**Fig. S7**). These results demonstrate that the *n*-back task exhibits multiple activation patterns as in the perceptual decision-making tasks (Experiments 1-3), but crucially, the nature of the activation patterns change with different underlying cognitive processes.

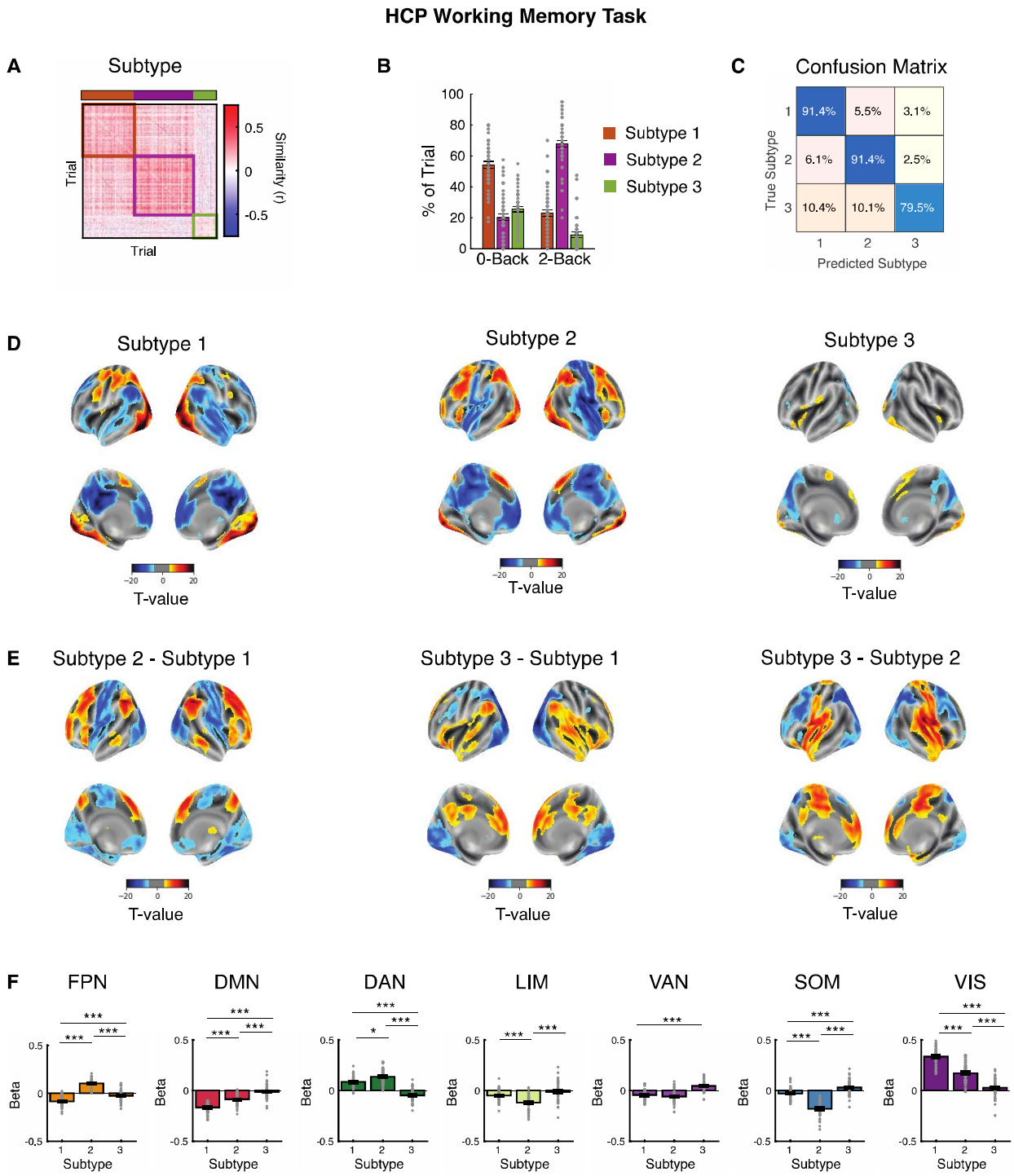

Figure 7. Subtypes of trials in an *n*-back task from the Human Connectome Project dataset. (A) Modularity-maximization clustering identified three subtypes of trials. The colored squares correspond to the trials composing each subtype. (B) The percent of trials classified as Subtype 1, 2, or 3 in the 0- and 2-back conditions. The bar graphs represent the average percent of trials across all individuals. The dots represent individual subjects. (C) Confusion matrix showing SVM classification accuracy between true and predicted subtypes from a 2-fold cross-

validation analysis. (D) Activation maps for each subtype. (E) Brain activation differences between subtypes. (F) Activation for each of seven large-scale brain networks for each subtype. The bar graph shows the average change in activation (mean ± sem). The grey dots show the activation in each subject. Brain maps are thresholded at $P_{FDR\text{-}corrected} < 0.01$. * $P_{FDR\text{-}corrected} < 0.05$, *** $P_{FDR\text{-}corrected} < 0.001$. FPN, Frontal Parietal Network; DMN, Default Mode Network; DAN, Dorsal Attention Network; LIM, Limbic Network; VAN, Ventral Attention Network; SOM, Somatomotor Network; VIS, Visual Network.

Processes underlying subtype activation

It is crucial to understand what brain or cognitive processes the subtypes could reflect and how their activation arises. Towards this end, we first determined the transition probabilities between subtypes similar to what might be done in Hidden-Markov models because such processes can result in clusters of trials exhibiting similar activation patterns. We found that in Experiments 1, 2 and the working memory task, the transition probabilities strongly deviated from random with strong re-occurrence of a subtype (**Fig. S8**). Additionally, we investigated a possible mechanism that would generate the multiple activation patterns from the structural or functional connectivity since both have been shown to be capable of predicting brain activation[24–26]. The result from the model suggest that global brain activation is primarily driven by the stimulus-drive from a few networks (see Supplementary Methods and Results for details and **Fig. S9-10**).

Subtypes are robust to methodological choices, experimental factors, and head motion

Finally, we examined whether the multiple activation patterns identified in each of the different tasks could be explained by methodological choices, experimental factors, or noise in the data (see Supplementary Results). First, in the main analyses, we estimated the similarity between trials based on voxel-wise activation, but voxel-wise estimates can be unstable and noisy. To account for this possibility, we repeated the analyses using activations within 200 brain regions and still found similar results (**Fig. S11**). Second, the number of clusters identified using modularity-maximization is dependent on the value of the resolution parameter (gamma). To determine that the obtained clusters are robust to this value, we additionally, re-ran the analysis using a range of gamma values (**Fig. S12)**. Third, the SVM analysis above relied on the same set of data for the training and testing. To ensure that the consistency results were not artificially inflated by this methodological choice, we confirmed the robustness of the subtypes in two additional SVM classification analyses that removed any overlap between the training and

testing data (**Fig. S13**). Further, we performed additionally analyses to confirm that factors including subject age and sex, trial position, or the time interval between successive trials were not driving the activation difference between trials (**Fig. S14-S15**). Lastly, we confirmed that the differences in activations between trials were not associated with motion-related artifacts (**Fig. S16-S19**). Collectively, we found that none of these factors plays a substantial role in determining the obtained subtypes.

Discussion

Fluctuations in brain activity are ubiquitous during simple and cognitively demanding tasks[27,28] and are often indicative of variation in cognitive processing[29]. However, meaningful variation in internal states that impacts cognition and behavior remains challenging to discover and characterize. Here we examined if distinct patterns of brain activity emerge on different trials when accomplishing the same task. We utilized a data-driven clustering method based on modularity-maximation to identify consistent patterns of brain activity on individual trials. Across three perceptual decision-making tasks, the clustering analysis identified multiple discrete subtypes of trials. Surprisingly, in each of the three experiments, one of the subtypes exhibited activations in DMN. To the best of our knowledge, this is the first analysis to report DMN activation on a subset of trials during a task that requires *externally focused* attention. Finally, we replicated the presence of multiple subtypes for a task that engages a different cognitive process (working memory). These findings demonstrate that the same task can be accomplished in the presence of widely varying brain activation patterns.

Our most striking finding was that trials from one of the subtypes in Experiments 1-3 showed a strong increase in DMN activity despite the fact that subjects were engaged in a perceptual decision-making task that canonically leads to DMN suppression. Behaviorally, the DMN-associated subtype was characterized by accuracy, RT, and confidence that were similar to the other subtypes associated with task-positive regions. These behavioral results are particularly surprising because DMN activation is usually associated with mind-wandering and being off-task[30,31]. It is important to note that DMN is known to be activated during task requiring internal or self-relevant focus[32–36] or boredom[37]. As a result, the activation of the DMN may reflect a change in attention from externally to internally focused attention or boredom. Yet such

interpretations would presumably predict larger behavioral differences between the DMN-associated subtype and the subtypes associated with increased activation in task-positive regions. Our findings demonstrate substantial DMN activations even for tasks that canonically should deactivate the DMN, which challenges the notion that DMN should be viewed as a task-negative network[38].

Why are multiple qualitatively different patterns of brain activity emerging from different trials of the same task? One may speculate that a cognitive process can be accomplished through multiple pathways. In fact, it has been hypothesized that multiple cognitive pathways could exist because of degeneracy[19], and this hypothesis is supported by work utilizing theoretical models and patient populations[20]. Similar to a person driving home from work, there may be multiple routes to get home and the path taken may depend on various factors such as the extent of traffic on a specific route. In this interpretation, the subtypes in perceptual decision-making tasks may be characterized as reflecting decision-making pathways in the presence of endogenous attention[39–41], exogenous attention[42,43], or internally focused attention[44]. In a similar manner, in the *n*-back task, the different subtypes could reflect engagement of different cognitive control mechanisms[45], maintenance[46], or action planning processes[47]. Note that the working memory task did not produce a subtype with DMN activations. It is thus an open question what tasks beyond perceptual decision making would show a DMN-associated subtype.

Instead of discrete pathways, another possibility is that the trial subtypes are part of a gradient in activation across the brain[48,49]. In this interpretation, the trial subtypes would indicate the axes of this space. Specifically, in the perceptual decision-making tasks, the location of an individual trial within this space could be dependent on the extent of top-down control[50,51], the salience of the stimulus[41], and internally oriented attention[52,53]. Critically, neither interpretation excludes the existence of shared components. Indeed, we found that the visual regions exhibited similar patterns in activation in all subtypes across all experiments. Additionally, this consistent pattern of activation included regions in the frontal, parietal, and temporal areas, suggesting a core component across all trials. Future research should examine the underlying processes that lead to the emergence of these trial subtypes across an array of cognitive functions.

In conclusion, we found that both perceptual decision-making and working memory tasks featured multiple distinct patterns of brain activation. These results suggest that several independent pathways may be employed to accomplish a task.

Methods

Experiment 1 Subjects and Task

Fifty healthy subjects (25 females; Mean age = 26; Age range = 19-40) that has been described elsewhere[54]. All subjects were screened for any history of neurological disorders or MRI contraindications. The study was approved by Ulsan National Institute of Science and Technology Review Board and all subjects gave written consent.

Subjects had to determine which set of colored dots (red vs. blue) is more frequent in a cloud of dots. Each trial began with a white fixation dot presented for a variable amount of time between 500-1500 ms. Then, the stimulus was shown for 500 ms, followed by untimed decision and confidence screens. The stimulus consisted of between 140 and 190 red- and blue-colored dots (dot size = 5 pixels) dispersed randomly inside an imaginary circle with a radius of 3° from the center of the screen. Four different dot ratios were used – 80/60, 80/70, 100/80, and 100/90, where the two numbers indicate the number of dots from each color. The luminance between the red and blue dots was not matched. Subjects performed a total of 768 trials. Three subjects completed only half of the 6th run and another three subjects completed only the first 5 runs due to time constraints. The remaining 44 subjects completed the full 6 runs.

Experiment 1 MRI Recording

The MRI data was collected on a 64-channel head coil 3T MRI system (Magnetom Prisma; Siemens). Whole-brain functional data were acquired using a T2*-weighted multi-band accelerated imaging (FoV = 200 mm; TR = 2000 ms; TE = 35 ms; multiband acceleration factor = 3; in-plane acceleration factor = 2; 72 interleaved slices; flip angle = 90°; voxel size = 2.0 x 2.0 x 2.0 mm^3). High-resolution anatomical MP-RAGE data were acquired using T1-weighted imaging (FoV = 256 mm; TR = 2300 ms; TE = 2.28 ms; 192 slices; flip angle = 8°; voxel size = 1.0 x 1.0 x 1.0 mm^3).

Experiment 2 Subjects and Task

Thirty-nine subjects (23 females, average age = 21.5 years, range = 18–28 years, compensated $50 for participation) were instructed to indicate whether a moving-dots stimulus had an overall coherent motion (always in downward direction) or not. Subjects had no history of

neurological disorders and had normal or corrected-to-normal vision. The study was approved by the Georgia Tech Institutional Review Board. All subjects were screened for MRI safety and provided informed consent. The study's method and procedure were carried out according to the declaration of Helsinki.

Detailed description can be found in Yeon et al[55]. In brief, each trial began with a fixation mark presented randomly for 1, 2, or 3 sec and followed by the stimulus presented for 500 ms. In the first half of the experiment (runs 1–3), subjects performed the task and were never told to evaluate their confidence level. In the second half of the experiment (runs 4–6), subjects made their perceptual decision and immediately after were asked to indicate their confidence level.

Experiment 2 MRI Recording

The MRI data were collected on 3T Prisma-Fit MRI system (Siemens) using a 32-channel head coil. Anatomical images were acquired using T1-weighted sequences (MEMPRAGE sequence, FoV = 256 mm; TR = 2530 ms; TE = 1.69 ms; 176 slices; flip angle = 7˚; voxel size = 1.0 × 1.0 × 1.0 mm^3). Functional images were acquired using T2*-weighted gradient echo-planar imaging sequences (FoV = 220 mm; TR = 1200 ms; TE = 30 ms; 51 slices; flip angle = 65˚; voxel size = 2.5 × 2.5 × 2.5 mm^3).

Experiment 3 Subjects and Task

The analysis was based on 40 subjects who performed a motion discrimination task. Subjects were compensated $20/hour or 1 course credit/hour for a total of 2.5 hours. All subjects were right-handed with normal hearing, normal or corrected-to-normal vision, had no history of neurological disorders, brain trauma, psychiatric illness, or illicit drug use. The study was approved by the Georgia Tech Institutional Review Board. All subjects were screened for MRI safety and provided written informed consent.

Detailed description can be found in Haddara & Rahnev[56]. In brief, subjects judged the motion direction (left or right) of white dots (density: 2 dots/degree², speed: 5°/s) presented in a black circle (3° radius) in front of a grey background. A proportion of dots moved coherently in the right or left direction while the rest of the dots moved randomly. Each dot motion stimulus was

preceded by a letter cue (“L” = Left, “R” = Right, “N” = Neutral). The letters L and R predicted the forthcoming stimulus with 75% validity, whereas the letter N was not predictive (both left and right motion were equally likely). Each trial began with cue presentation for 2, 4, or 6 seconds (chosen randomly), followed by a 3-second dot motion stimulus and an untimed response. A screen with a fixation dot was then presented between trials for a period of 1 or 2 seconds.

Experiment 3 MRI Recording

BOLD fMRI signal data was collected on a 3T MRI system (Prisma-Fit MRI system; Siemens) using a 32-channel head coil. Anatomical images were acquired using T1-weighted sequences (MEMPRAGE sequence, FoV = 256 mm; TR = 2530 ms; TE = 1.69 ms; 176 slices; flip angle = 7˚; voxel size = 1.0 x 1.0 x 1.0). Functional images were acquired using T2*-weighted gradient echo-planar imaging sequences (FoV = 220 mm; slice thickness = 2.5, TR = 1200 ms; TE = 30 ms; 51 slices; flip angle = 65˚; voxel size = 2.5 x 2.5 x 2.5, multi band factor = 3, interleaved slices).

HCP Working Memory Task

The analysis utilized the minimally preprocessed n-back data collected part of the Human Connectome Project[21]. Specifically, the analysis utilized WM_RL data in which each subjects completed 40 trials of 0- and 2-back trials. MRI scanning was done using a customized 3□T Siemens Connectome Skyra using a standard 32-channel Siemens receive head coil and a body transmission coil. T1-weighted high resolution structural images acquired using a 3D MPRAGE sequence with 0.7□mm isotropic resolution (FOV□=□224□mm, matrix□=□320, 256 sagittal slices, TR□=□2400□ms, TE□=□2.14□ms, TI□=□1000□ms, FA□=□8°). Working Memory fMRI data were collected using gradient-echo echo-planar imaging (EPI) with 2.0□mm isotropic resolution (FOV□=□208□×□180□mm, matrix□=□104□×□90, 72 slices, TR□=□720□ms, TE□=□33.1□ms, FA□=□52°, multi-band factor□=□8, 1200 frames, ~15□min/run).

Prior to estimating the task-induced brain activity on individual trials, the fMRI files were spatial smoothed with 10 mm full width half maximum (FWHM) Gaussian kernel. Task-induced brain activity in each voxel was estimated using GLMsingle[22]. Additionally, global signal and motion

parameters were included as factors in GLMsingle. For clustering, we pooled trials across subjects and *n*-back conditions (N_{subj} = 48; N_{trials} = 3840) in the same manner as in the perceptual decision-making tasks.

Experiment 1-3 MRI Preprocessing

MRI data were preprocessed with SPM12 (Wellcome Department of Imaging Neuroscience, London, UK). We first converted the images from DICOM to NIFTI and removed the first three volumes to allow for scanner equilibration. We then preprocessed with the following steps: de-spiking, slice-timing correction, realignment, segmentation, coregistration, normalization, and spatial smoothing with 10 mm full width half maximum (FWHM) Gaussian kernel except for Experiment 3 where smoothing was performed with a 6 mm FWHM Gaussian kernel. Despiking was done using the 3dDespike function in AFNI. The preprocessing of the T1-weighted structural images involved skull-removal, normalization into MNI anatomical standard space, and segmentation into gray matter, white matter, and cerebral spinal fluid, soft tissues, and air and background.

Single-Trial Beta Estimation

Single-trial beta responses were estimated with a general linear model (GLM) using GLMsingle, a Matlab toolbox for single-trial analyses[22]. The hemodynamic response function was estimated for each voxel and nuisance regressors were derived in the same manner as previously described in Allen et al.[57]. Additionally, regressors for the global signal and for six motion parameters (three translation and three rotation) were included. The single-trial betas were estimated in three batches. In each batch, the betas for every third trial were estimated because the trials in our study were temporally close together. Also, trials that were within 20 seconds from the end of run were removed. The betas for each voxel represent the estimated trial-wise BOLD response and are relative to the BOLD signal observed during the absence of the stimulus[22].

Modularity-maximization Based Clustering

The beta maps per trials were pooled among subjects to ensure that there was consistency in clustering correspondence. A trial-by-trial similarity matrix was created using the Pearson Product Correlation using all gray-matter voxels, except in the working memory task where all

brain voxels were used. Clustering of the similarity matrix was conducted using modularity-maximization[58]. Modularity-maximization does not require the number of clusters to be specified and the resolution of the clusters was controlled with resolution parameter, $\gamma = 1$. Modularity-maximization was implemented with the Generalized Louvain algorithm part of the Brain Connectivity Toolbox[59]. Clustering results from the Generalized Louvain algorithm can be dependent on the initial seeding. Therefore, clustering was repeated 100x with different initial seeds, and final clustering results were based on the consensus across iterations[60]. Specifically, consensus clustering identifies a single representative partition from the set of 100 iterations. This process involves the creation of a thresholded nodal association matrix which describes how often nodes were placed in the same cluster. The representative partition is then obtained by using a Generalized Louvain algorithm to identify clusters within the thresholded nodal association matrix[60]. We have previously utilized this method to identify trial subtypes in brain activity measured with electroencephalography in a motion discrimination[61] task and working memory task[62].

To ensure that the number of clusters was not dependent on the value of the resolution parameter (gamma), we re-ran the clustering with gamma values ranging from 0.8 to 1.2. A value of 1 for the resolution parameter is considered standard[63], which is why we used it. However, increasing gamma favors the identification of smaller clusters and lowering gamma favors the identification of larger clusters. Further, we expected to find a small number of clusters because in previous work in which we clustered trials in EEG data we found at most three[62,64].

Standard Group-Level Analysis

A standard task-based GLM analysis was conducted to identify voxels in which the beta values significantly deviated from zero. Specifically, a single activation brain map was created per subject by averaging the individual beta maps across trials and a one-sample t-tests was conducted across subjects to identify the regions that deviated from zero.

Trial Subtype Activation

In a similar manner to the standard group-level analysis, a trial subtype task-based analysis was conducted to identify voxels in which the beta values for each subtype of trials significantly

deviated from zero. For each subtype, a single activation brain map was created per subject by averaging the individual beta maps across trials in each subtype. A group-level one-sample t-tests was conducted to identify voxels with significant increase or decrease in activation. Activation maps were false discovery rate (FDR) corrected for multiple comparison.

Standard General Linear Modeling

To further corroborate the results, we also performed a standard GLM using SPM12 with subtypes as factors in the regression and found similar patterns of activations. We fit a GLM that allowed us to estimate the beta values for each voxel in the brain in each of the trial subtypes. The model consisted of separate regressors for each of the subtypes, inter-block rest periods, as well as linear and squared regressors for six motion parameters (three translation and three rotation), five tissue-related regressors (gray matter, white matter, and cerebrospinal fluid), global signal, and a constant term per run.

Consistency in Activation Across Subtypes

To identify voxels exhibiting consistent task-induced changes in brain activity, we examined the consistency of the sign of voxel activations (positive or negative) across subjects. To do so, for each of the subtype brain maps, we first removed all non-gray matter voxels. We then binarized the voxel activation values $activation_i$ such that:

$$binary_i = \begin{cases} 1, & activation_i > 0 \\ -1, & activation_i < 0 \end{cases}$$

The consistency of the sign of a voxel's activation across subtypes (C_i) was then calculated as total number of subtypes for a which voxel i was positively or negatively activated using the formula:

$$C_i = \sum_{i=1}^{3} binary_i$$

As defined, C_i goes from -3 (all subtypes having negative activation for that voxel) to 3 (all subtypes having positive activations for that voxel). C_i was then thresholded at ± 3 to identify voxels that consistently increased or decreased in brain activity across subtypes. The brain maps where then averaged across subjects.

Voxel and Brain Network Differences Between Subtypes

Differences in task-based brain activity between subtypes was conducted to identified voxels in which the beta values between subtypes differed. The analysis was conducted both at the voxelwise and between large-scale brain networks. For voxelwise analyses, a paired t-test was used to test for differences between subtypes. For the comparison between large-scale brain networks, the beta values from voxels associated with one of seven large-scale brain networks part of the Schaefer Atlas[23] were averaged together within a subject and a paired t-test was used to test for differences between subtypes. All p-values were false discovery rate (FDR) corrected for multiple comparison.

Behavioral Performance Differences Between Subtypes

A linear mixed-effect model was used to test for differences in accuracy, RT and confidence between subtypes. The model assessed the effects of subtype and condition with the subject as a random factor on behavioral performance.

Brain-Behavior Relationship Within Each Subtype Compared to Across All Trials

To test if clustering trials improved the brain-behavior relationship estimation, we estimated the brain-behavior in each subtype and compared it to all trial pooled together. Specifically, we calculated the average activation in each brain region part of the Schaefer 200 brain atlas. Within each subject, for each region we correlated the trial activation strength with accuracy, RT and confidence for each subtype of trials and all trials together. We estimated the change in sensitivity in the brain-behavior relationship as:

$$\Delta\, Sensitivity_{i,k} = \left|r_{act_{i,k},beh_{i,k}}\right| - \left|r_{act_{i,all},beh_{i,all}}\right|$$

where $\left|r_{act_{i,k},beh_{i,k}}\right|$ is the absolute value of the correlation for trials in subtype k between activation strength in brain region i and behavioral performance and $\left|r_{act_{i,all},beh_{i,all}}\right|$ is the absolute value in correlation between activation strength in brain region i and behavioral performance across all trials.

SVM Classification

A 2-fold cross-validation analysis using Support Vector Machine (SVM) classifier was performed with MATLAB's *fitcecoc.m.* We opted for a two-fold cross validation because the two-fold separation provides a balance between the number of trials used for training and testing while minimizing the possibility of overfitting to the data. Trials were randomly separated into two bins containing 50% of trials each. The SVM classifier was trained on the first bin of trials and tested on the second bin. The procedure was repeated with the training and testing bins swapped. Classification accuracy was computed by comparing the predicated to the empirical trial subtype label.

We performed two additional SVM classification analyses. For the first analysis, an SVM model was trained on data from half the of the subject and tested on the data from the remaining subjects. This separation ensured that any effects that might have spanned across trials within a subject do not affect the data used for testing. Critically, splitting the data based on subjects provides an initial assessment of how well subtypes can be translated to data from new subjects in future studies. In the second analysis, we similarity split the subjects in half but then repeated the clustering analysis on each half and trained an SVM classifier to predict the labels on the data from the other half of subjects. This analysis tests whether labels can be predicted on trials that were not included in the clustering.

Transition Probabilities

We calculated transition probabilities by computing the probability of a trial from each subtype to be followed by a trial from any subtype.

Data and Code Availability

The analysis was based on a combination of publicly available toolboxes, datasets and analysis specific scripts. Specifically, single-trial betas were estimated using GLMsingle and is available at https://github.com/cvnlab/GLMsingle. Clustering analysis was based on the Community Louvain part of the Brain Connectivity Toolbox (https://sites.google.com/site/bctnet/)[59]. Consensus clustering was determined using *consensus_iterative.m*

(http://commdetect.weebly.com/). Brain maps and scripts required to conduct the analysis are available will be made available upon publication.

References

1. Arieli, A., Sterkin, A., Grinvald, A. & Aertsen, A. Dynamics of ongoing activity: Explanation of the large variability in evoked cortical responses. *Science (1979)* (1996) doi:10.1126/science.273.5283.1868.
2. Goris, R. L. T., Movshon, J. A. & Simoncelli, E. P. Partitioning neuronal variability. *Nat Neurosci* (2014) doi:10.1038/nn.3711.
3. Ribrault, C., Sekimoto, K. & Triller, A. From the stochasticity of molecular processes to the variability of synaptic transmission. *Nature Reviews Neuroscience* Preprint at https://doi.org/10.1038/nrn3025 (2011).
4. Clare Kelly, A. M., Uddin, L. Q., Biswal, B. B., Castellanos, F. X. & Milham, M. P. Competition between functional brain networks mediates behavioral variability. *Neuroimage* (2008) doi:10.1016/j.neuroimage.2007.08.008.
5. Reinhart, R. M. G. & Nguyen, J. A. Working memory revived in older adults by synchronizing rhythmic brain circuits. *Nat Neurosci* **22**, 820–827 (2019).
6. Mišić, B., Mills, T., Taylor, M. J. & McIntosh, A. R. Brain Noise Is Task Dependent and Region Specific. *J Neurophysiol* **104**, 2667–2676 (2010).
7. Durlauf, S. N. A framework for the study of individual behavior and social interactions. *Sociol Methodol* **31**, (2001).
8. Kable, J. W. & Glimcher, P. W. The neural correlates of subjective value during intertemporal choice. *Nat Neurosci* **10**, (2007).
9. Afraz, A., Pashkam, M. V. & Cavanagh, P. Spatial heterogeneity in the perception of face and form attributes. *Current Biology* **20**, (2010).
10. Friston, K. J., Holmes, A. P., Price, C. J., Büchel, C. & Worsley, K. J. Multisubject fMRI Studies and Conjunction Analyses. *Neuroimage* **10**, 385–396 (1999).
11. Kanwisher, N., McDermott, J. & Chun, M. M. The Fusiform Face Area: A Module in Human Extrastriate Cortex Specialized for Face Perception. *The Journal of Neuroscience* **17**, 4302 LP – 4311 (1997).
12. Christophel, T. B., Klink, P. C., Spitzer, B., Roelfsema, P. R. & Haynes, J.-D. The Distributed Nature of Working Memory. *Trends Cogn Sci* **21**, 111–124 (2017).
13. Patai, E. Z. & Spiers, H. J. The Versatile Wayfinder: Prefrontal Contributions to Spatial Navigation. *Trends Cogn Sci* **25**, 520–533 (2021).
14. Spiers, H. J. & Maguire, E. A. A navigational guidance system in the human brain. *Hippocampus* **17**, 618–626 (2007).
15. Fox, M. D. *et al.* The human brain is intrinsically organized into dynamic, anticorrelated functional networks. *Proc Natl Acad Sci U S A* (2005) doi:10.1073/pnas.0504136102.
16. Garrett, D. D. *et al.* Moment-to-moment brain signal variability: A next frontier in human brain mapping? *Neurosci Biobehav Rev* **37**, 610–624 (2013).
17. Waschke, L., Wöstmann, M. & Obleser, J. States and traits of neural irregularity in the age-varying human brain. *Sci Rep* **7**, 17381 (2017).

18. McIntosh, A. R., Kovacevic, N. & Itier, R. J. Increased Brain Signal Variability Accompanies Lower Behavioral Variability in Development. *PLoS Comput Biol* **4**, e1000106- (2008).
19. Tononi, G., Sporns, O. & Edelman, G. M. Measures of degeneracy and redundancy in biological networks. *Proceedings of the National Academy of Sciences* **96**, 3257–3262 (1999).
20. Sajid, N., Parr, T., Hope, T. M., Price, C. J. & Friston, K. J. Degeneracy and redundancy in active inference. *Cerebral Cortex* **30**, 5750–5766 (2020).
21. Barch, D. M. *et al.* Function in the human connectome: Task-fMRI and individual differences in behavior. *Neuroimage* **80**, 169–189 (2013).
22. Prince, J. S. *et al.* Improving the accuracy of single-trial fMRI response estimates using GLMsingle. *Elife* **11**, e77599 (2022).
23. Schaefer, A. *et al.* Local-Global Parcellation of the Human Cerebral Cortex from Intrinsic Functional Connectivity MRI. *Cerebral Cortex* **28**, 3095–3114 (2018).
24. Deco, G. *et al.* Resting-State Functional Connectivity Emerges from Structurally and Dynamically Shaped Slow Linear Fluctuations. *The Journal of Neuroscience* **33**, 11239 (2013).
25. Goni, J. *et al.* Resting-brain functional connectivity predicted by analytic measures of network communication. *Proceedings of the National Academy of Sciences* **111**, 833–838 (2014).
26. Honey, C. J. *et al.* Predicting human resting-state functional connectivity from structural connectivity. *Proceedings of the National Academy of Sciences* (2009) doi:10.1073/pnas.0811168106.
27. Garrett, D. D. *et al.* Moment-to-moment brain signal variability: A next frontier in human brain mapping? *Neurosci Biobehav Rev* **37**, 610–624 (2013).
28. Faisal, A. A., Selen, L. P. J. & Wolpert, D. M. Noise in the nervous system. *Nat Rev Neurosci* **9**, 292–303 (2008).
29. Waschke, L., Kloosterman, N. A., Obleser, J. & Garrett, D. D. Behavior needs neural variability. *Neuron* **109**, 751–766 (2021).
30. Christoff, K., Irving, Z. C., Fox, K. C. R., Spreng, R. N. & Andrews-Hanna, J. R. Mind-wandering as spontaneous thought: a dynamic framework. *Nat Rev Neurosci* **17**, 718–731 (2016).
31. Mason, M. F. *et al.* Wandering Minds: The Default Network and Stimulus-Independent Thought. *Science (1979)* **315**, 393–395 (2007).
32. Grady, C. L. & Garrett, D. D. Brain signal variability is modulated as a function of internal and external demand in younger and older adults. *Neuroimage* **169**, 510–523 (2018).
33. Grigg, O. & Grady, C. L. The default network and processing of personally relevant information: converging evidence from task-related modulations and functional connectivity. *Neuropsychologia* **48**, 3815–3823 (2010).
34. Andrews-Hanna, J. R., Reidler, J. S., Sepulcre, J., Poulin, R. & Buckner, R. L. Functional-anatomic fractionation of the brain's default network. *Neuron* **65**, 550–562 (2010).

35. Buckner, R. L. & Carroll, D. C. Self-projection and the brain. *Trends Cogn Sci* **11**, 49–57 (2007).
36. Buckner, R. L., Andrews-Hanna, J. R. & Schacter, D. L. The brain's default network: anatomy, function, and relevance to disease. *Ann N Y Acad Sci* **1124**, 1–38 (2008).
37. Danckert, J. & Merrifield, C. Boredom, sustained attention and the default mode network. *Exp Brain Res* **236**, 2507–2518 (2018).
38. Spreng, R. N. The Fallacy of a "Task-Negative" Network . *Frontiers in Psychology* vol. 3 Preprint at https://www.frontiersin.org/articles/10.3389/fpsyg.2012.00145 (2012).
39. Dosenbach, N. U. F. *et al.* Distinct brain networks for adaptive and stable task control in humans. *Proceedings of the National Academy of Sciences* **104**, 11073–11078 (2007).
40. Spreng, R. N., Stevens, W. D., Chamberlain, J. P., Gilmore, A. W. & Schacter, D. L. Default network activity, coupled with the frontoparietal control network, supports goal-directed cognition. *Neuroimage* **53**, 303–317 (2010).
41. Corbetta, M. & Shulman, G. L. Control of goal-directed and stimulus-driven attention in the brain. *Nat Rev Neurosci* **3**, 201–215 (2002).
42. Sridharan, D., Levitin, D. J. & Menon, V. A critical role for the right fronto-insular cortex in switching between central-executive and default-mode networks. *Proc Natl Acad Sci U S A* **105**, 12569–12574 (2008).
43. Seeley, W. W. *et al.* Dissociable intrinsic connectivity networks for salience processing and executive control. *Journal of Neuroscience* **27**, 2349–2356 (2007).
44. Buckner, R. L. & DiNicola, L. M. The brain's default network: updated anatomy, physiology and evolving insights. *Nat Rev Neurosci* **20**, 593–608 (2019).
45. Braver, T. S. The variable nature of cognitive control: a dual mechanisms framework. *Trends Cogn Sci* **16**, 106–113 (2012).
46. Miller, E. K., Lundqvist, M. & Bastos, A. M. Working Memory 2.0. *Neuron* **100**, 463–475 (2018).
47. Boettcher, S. E. P., Gresch, D., Nobre, A. C. & van Ede, F. Output planning at the input stage in visual working memory. *Sci Adv* **7**, eabe8212 (2024).
48. Margulies, D. S. *et al.* Situating the default-mode network along a principal gradient of macroscale cortical organization. *Proceedings of the National Academy of Sciences* **113**, 12574–12579 (2016).
49. Tian, Y., Margulies, D. S., Breakspear, M. & Zalesky, A. Topographic organization of the human subcortex unveiled with functional connectivity gradients. *Nat Neurosci* **23**, 1421–1432 (2020).
50. Cole, M. W. *et al.* Multi-task connectivity reveals flexible hubs for adaptive task control. *Nat Neurosci* **16**, 1348–1355 (2013).
51. Koechlin, E., Ody, C. & Kouneiher, F. The Architecture of Cognitive Control in the Human Prefrontal Cortex. *Science (1979)* **302**, 1181–1185 (2003).
52. Rosenberg, M. D. *et al.* A neuromarker of sustained attention from whole-brain functional connectivity. *Nat Neurosci* **19**, (2015).

53. Kucyi, A., Hove, M. J., Esterman, M., Hutchison, R. M. & Valera, E. M. Dynamic Brain Network Correlates of Spontaneous Fluctuations in Attention. *Cerebral Cortex* **27**, 1831–1840 (2017).
54. Nakuci, J. *et al.* Quantifying the idiosyncrasy in brain activations. *bioRxiv* 2022.08.01.502338 (2023) doi:10.1101/2022.08.01.502338.
55. Yeon, J., Shekhar, M. & Rahnev, D. Overlapping and unique neural circuits are activated during perceptual decision making and confidence. *Sci Rep* **10**, (2020).
56. Haddara, N. & Rahnev, D. Threat expectation does not improve perceptual discrimination despite causing heightened priority processing in the frontoparietal network. *bioRxiv* (2023).
57. Allen, E. J. *et al.* A massive 7T fMRI dataset to bridge cognitive neuroscience and artificial intelligence. *Nat Neurosci* **25**, 116–126 (2022).
58. Mucha, P. J., Richardson, T., Macon, K., Porter, M. A. & Onnela, J. P. Community structure in time-dependent, multiscale, and multiplex networks. *Science (1979)* (2010) doi:10.1126/science.1184819.
59. Rubinov, M. & Sporns, O. Complex network measures of brain connectivity: Uses and interpretations. *Neuroimage* **52**, 1059–1069 (2010).
60. Bassett, D. S. *et al.* Robust detection of dynamic community structure in networks. *Chaos* (2013) doi:10.1063/1.4790830.
61. Nakuci, J., Samaha, J. & Rahnev, D. Brain signatures indexing variation in internal processing during perceptual decision-making. *bioRxiv* 2023.01.10.523502 (2023) doi:10.1101/2023.01.10.523502.
62. Nakuci, J., Covey, T. J., Shucard, J. L., Shucard, D. W. & Muldoon, S. F. Single trial variability in neural activity during a working memory task reveals multiple distinct information processing sequences. *Neuroimage* **269**, 119895 (2023).
63. Porter, M. A., Onnela, J.-P. & Mucha, P. J. Communities in networks. (2009).
64. Nakuci, J., Samaha, J. & Rahnev, D. Brain signatures indexing variation in internal processing during perceptual decision-making. *iScience* **26**, (2023).